Principal Modes of Diurnal Cycle of Rainfall over South China during the Presummer Rainy Season

FU DONG,[a] XIEFEI ZHI,[a,b] SHOUPENG ZHU,[c] LING ZHANG,[a] FEI GE,[d] YI FAN,[a] YANG LYU,[a] JINGYU WANG,[e] AND KLAUS FRAEDRICH[a,f]

[a] *Key Laboratory of Meteorology Disaster, Ministry of Education/Joint International Research Laboratory of Climate and Environment Change/Collaborative Innovation Center on Forecast and Evaluation of Meteorological Disasters, Nanjing University of Information Science and Technology, Nanjing, China*
[b] *WeatherOnline (Wuxi) Science and Technology Co. Ltd., Wuxi, China*
[c] *China Meteorological Administration Transportation Meteorology Key Laboratory/Nanjing Joint Institute for Atmospheric Sciences, Nanjing, China*
[d] *School of Atmospheric Sciences/Plateau Atmosphere and Environment Key Laboratory of Sichuan Province/ Joint Laboratory of Climate and Environment Change, Chengdu University of Information Technology, Chengdu, China*
[e] *National Institute of Education, Nanyang Technological University, Singapore*
[f] *Max Planck Institute for Meteorology, Hamburg, Germany*

(Manuscript received 23 April 2022, in final form 25 November 2022)

ABSTRACT: The principal modes of the diurnal cycle of rainfall (DCR) over South China during the presummer rainy season are examined using 23-yr satellite observations and reanalysis data. Three distinctly different DCR modes are identified via empirical orthogonal function analysis, that is, the early-afternoon precipitation (EAP) mode, the late-afternoon precipitation (LAP) mode, and the morning precipitation (MP) mode. Under the EAP mode, the rainfall starts to increase from midnight and reaches its peak in the early afternoon. The nocturnal to morning rainfall generally concentrates on the northeastern Pearl River delta (PRD) and along the coastline. The coastal rainfall is initiated from the convergence zone induced by the strong onshore wind and is further enhanced via the establishment of a land breeze in the early morning. The northeastern PRD center is mainly attributed to the windward mechanical lifting associated with the strong low-level wind. The afternoon rainfall is pronounced over inland areas and exhibits significantly regional diversity. The eastern inland rainfall develops from the early-morning rainfall over the northeastern PRD, whereas the eastward-propagating rain belts associated with frontal activities are responsible for the formation of western inland rainfall. The LAP mode features a late-afternoon peak, which is triggered and developed locally with favorable thermal–dynamic conditions over western inland South China. The MP mode exhibits a single early-morning peak. Nocturnal to morning rainfall is prominent on the northeastern PRD and near-offshore region. The near-offshore rainfall is basically induced by the convergence between the onshore wind and land breeze in the early morning, which further propagates far offshore in the morning due to effects of gravity waves.

KEYWORDS: Diurnal effects; Jets; Rainfall; Wind; Empirical orthogonal functions

1. Introduction

The diurnal cycle of rainfall (DCR) is an important aspect of the global climate system and has been extensively studied for several decades (Wallace 1975; Yang and Slingo 2001; Dai 2001; Wang et al. 2011). The DCR exhibits pronounced regional and seasonal variations owing to the variety of the thermal and dynamic process and inhomogeneous surface types (Dai et al. 1999; Kikuchi and Wang 2008; Li et al. 2008; Yuan et al. 2012). Understanding the spatiotemporal features of the DCR and the underlying physical mechanisms is not only important to predict the regional rainfall, but it is also necessary to further enhance the capability of disaster prevention and reduction (Dai and Trenberth 2004; Li et al. 2018; Cai et al. 2021; Zhang et al. 2022).

South China, located at the north of the South China Sea (SCS) and southeast of the Yunnan Guizhou Plateau (YGP) (Fig. 1a), is one of the rainfall centers over East Asia. Yu et al. (2007b) investigated the DCR during the summer over South China using hourly rain gauge data, suggesting a single afternoon peak of the local rainfall. Based on the high-resolution gauge-satellite merged data, Jiang et al. (2017) further revealed double peak features of the DCR over South China, with a major peak in the afternoon and a secondary early-morning peak. Using fine-scale rain gauge data and satellite data, Chen et al. (2018) examined the DCR over South China and found that the morning rainfall is pronounced near the coast and windward mountains, while the afternoon rainfall dominants over the land. The features of rainfall over South China are distinctly different between in the morning and afternoon, in terms of rainfall duration, frequency, intensity and propagation. The long-duration rainfall events tend to reach the maximum in the early morning, while short-duration events peak in the late afternoon (Yu et al. 2007a). The morning rainfall features larger intensity but smaller frequency compared with that in the afternoon (Jiang et al. 2017; Li et al. 2018). The

Supplemental information related to this paper is available at the Journals Online website: https://doi.org/10.1175/JCLI-D-22-0284.s1.

Corresponding author: Xiefei Zhi, zhi@nuist.edu.cn

DOI: 10.1175/JCLI-D-22-0284.1

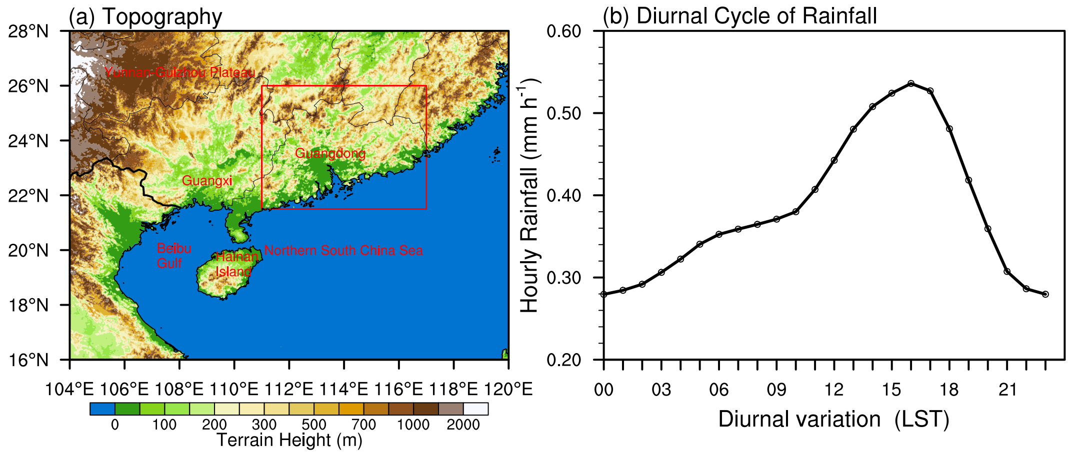

FIG. 1. (a) Topographic (m) map of South China. South China is defined in this study as the region within the red box (21.5°–26°N, 111°–117°E). (b) Diurnal cycle of mean hourly rainfall (mm h^{-1}) over South China during the presummer rainy season.

nocturnal to morning rainfall near the coast exhibits an offshore propagating mode, whereas the inland afternoon rainfall is quasi-stationary (Chen et al. 2015; Jiang et al. 2017; Bai et al. 2020).

The DCR associated mechanisms have been widely proposed for South China. The low-level monsoonal wind, with its peak at late night or in the early morning, strongly dominates the spatial and diurnal patterns of rainfall (Chen et al. 2009, 2013; Bai et al. 2021). Such a diurnal monsoon variability exhibits seasonal, interannual and interdecadal variations, and acts as a key regional process regulating the rainfall over East Asia (Chen et al. 2021). On the synoptic scale, the low-level jet (LLJ) is important for the horizontal distribution and diurnal variation of rainfall over South China by transporting warm–moist air with a convergence at their termini (Stensrud 1996; Du and Chen 2019b). In particular, LLJs over South China and the adjacent area can be classified into two types: boundary layer jets (BLJs) occurring below the level of 1 km; and synoptic-weather-related LLJs, which are observed at levels of 1–4 km (Du et al. 2014). Both the BLJs and synoptic-weather-related LLJs show pronounced diurnal variations and play crucial roles in regulating the nocturnal to morning rainfall (Jiang et al. 2017; Du and Chen 2019a). Dong et al. (2021) further revealed the important impacts of BLJs over the northern SCS and Beibu Gulf on the afternoon rainfall over South China. In addition, the controlling role of the land–sea breeze in the DCR over the South China coastal region has been widely discussed (Chen et al. 2015, 2016; Su et al. 2021). The near offshore rainfall over South China has been revealed to be closely related to the convergence of the onshore monsoonal wind and the land breeze, while the daytime inland-penetrating precipitation is mainly produced by the intrusion of sea-breeze fronts (Chen et al. 2016, 2017). Besides, the effect of gravity waves is also one of the key factors responsible for the offshore propagation modes near the South China coast (Aves and Johnson 2008; Du and Rotunno 2018; Bai et al. 2020).

Such multiscale factors modulating rainfall over South China have been demonstrated conspicuously from May to June, which is often referred to as the presummer rainy season (Huang 1986). The presummer rainy season is the major rainy season over South China, whose rainfall amount accounts for 40%–50% of the local annual rainfall (Huang 1986; Ding 1992). In addition, the presummer rainfall over South China appears to be characterized by extensive complexities of the DCR (Chen et al. 2015; Jiang et al. 2017; Wang et al. 2021; Dong et al. 2021), which have not yet been comprehensively revealed. Therefore, it is necessary to make further classifications and to investigate their spatiotemporal variabilities jointly with the controlling mechanisms. The purposes of this study are to identify the principal modes of the DCR over South China during the presummer rainy season and to examine the underlying mechanisms controlling the DCR under different modes.

The next section introduces the datasets and methodology employed in the present study. Section 3 identifies principal modes of the DCR over South China and presents the rainfall characteristics under different modes. The possible mechanisms modulating the DCR associated with the principal modes are analyzed in section 4. A summary and discussion are given in the final section.

2. Data and methodology

The Climate Prediction Center morphing technique (CMORPH) global precipitation dataset (Joyce et al. 2004) is used as observations with the spatial and temporal resolutions of 8 km and 30 min, respectively. The half-hourly CMORPH data are processed to hourly records in this study. Previous literatures have illustrated its considerable capability of reflecting the DCR characteristics over South China (Chen et al. 2018; Du and Rotunno 2018). The latest European Centre for Medium-Range Weather Forecasts (ECMWF) reanalysis ERA5 (Hersbach et al. 2020) with 0.25° × 0.25° grids at 1 h intervals is used to diagnose the atmospheric conditions. The

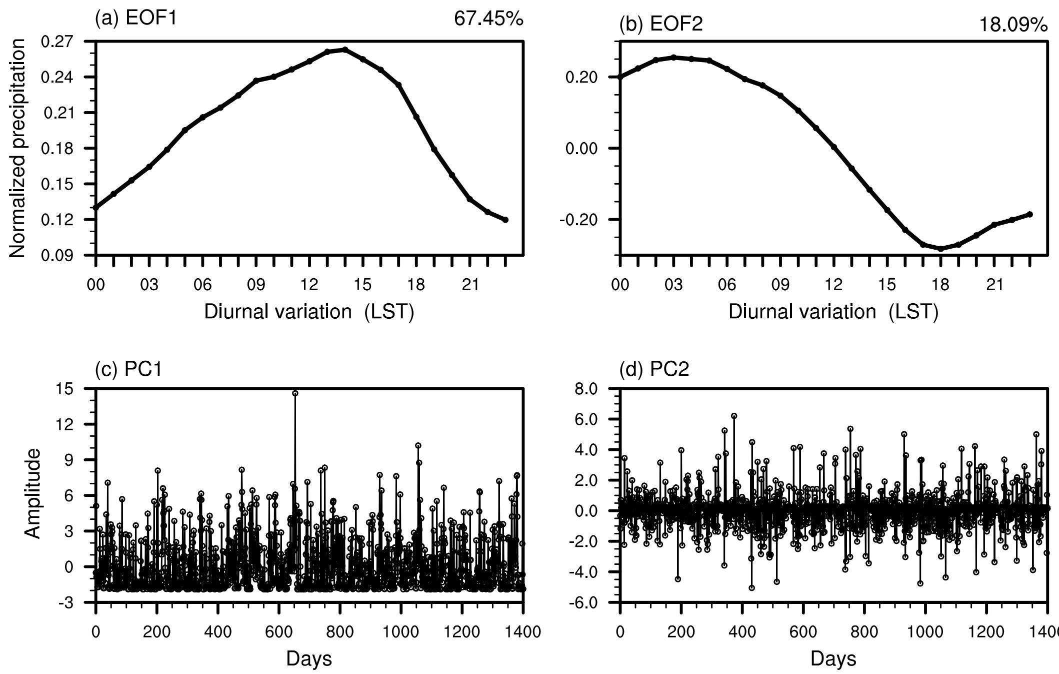

FIG. 2. (a),(b) The diurnal patterns of the first two EOF modes. (c),(d) Time series of the principal components PC1 and PC2.

analyses conducted in this study are performed for the presummer rainy season (May–June) from 1998 to 2020.

In this study, the empirical orthogonal function (EOF) analysis is employed to obtain the principal modes of the DCR over South China during the presummer rainy season. The EOF method is always a powerful tool to detect the variable spatiotemporal characteristics, which has been demonstrated to work well to identify the prominent diurnal harmonics modes in satellite data and models (Kikuchi and Wang 2008; Wang et al. 2011). The EOF analysis is performed toward the normalized (by the daily mean) diurnal rainfall dataset averaged over South China (the red box in Fig. 1a) with a metric size of 24 [from 0000 to 2300 local standard time (LST)] $\times$ 1403 (23-yr presummer days). Results are shown in the following section.

3. The principal modes of diurnal cycle of rainfall

According to the DCR over South China during the presummer rainy season (Fig. 1b), rainfall exhibits a double peak feature, that is, a major afternoon peak ($\sim$1600 LST) and a secondary morning peak ($\sim$0600 LST). The precipitation is lowest at around midnight. Such features have been widely validated in previous literatures (Jiang et al. 2017; Chen et al. 2018; Dong et al. 2021). Figures 2a and 2b present the first two leading EOF modes of the DCR, which account for 67.45% and 18.09% of the total variance, respectively. The EOF3 accounts for less than 10% of the total variance and would not be further discussed in this study. The EOF1 exhibits a double-peak feature, with a major peak at 1400 LST and a secondary peak at around 0900 LST. The precipitation increases from nocturnal to early afternoon, while decreases after 1400 LST (Fig. 2a). Thus, the EOF1 mode is hereafter named the early-afternoon precipitation (EAP) mode. The positive EOF2 signal represents a single early-morning peak ($\sim$0300 LST) with a minimum around 1800 LST, exhibiting pronounced morning rainfall and negligible afternoon rainfall. Hence, this mode is referred to as the morning precipitation (MP) mode. On the contrary, the negative EOF2 signal shows an afternoon peak at 1800 LST and will be called the late-afternoon precipitation (LAP) mode.

To distinguish the different DCR modes in more detail, the days with a significant DCR under the above three modes are further identified. Days with PC1 magnitudes of greater than one standard deviation are selected as the EAP days (Fig. 2c). Similarly, days with positive and negative PC2 magnitudes greater than one standard deviation are identified as the MP and LAP days, respectively (Fig. 2d). It is worth noting that the duplicate days will be classified as the EAP (MP and LAP) days when the PC1 (positive and negative PC2) exhibits the highest amplitude among the above three PC patterns. Based on the above criteria, a total of 173 EAP days, 126 LAP days, and 85 MP days are selected and no overlapping days exist among the identified modes. The spatial patterns of composite hourly rainfall during the EAP, LAP, and MP days are shown in Fig. 3. The following results are noted:

(i) For the EAP days, rainfall initializes at around midnight over the northeastern Pearl River delta (PRD) and along the coast (Fig. 3a) and further strengthens in the early morning (Figs. 3b–d). The coastal rainfall propagates offshore in the morning, with a speed of around 6 m s^{-1} (Fig. 4a). Besides, the rainfall along the coastline

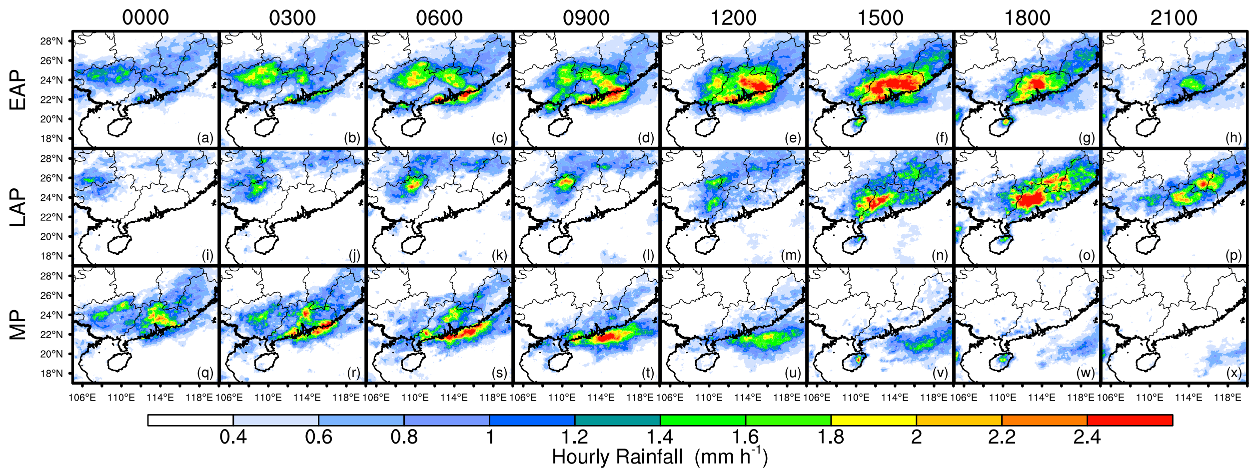

FIG. 3. The composite hourly rainfall (mm h^{-1}) from 0000 to 2100 LST with the 3-h interval derived from CMORPH during the (a)–(h) EAP, (i)–(p) LAP, and (q)–(x) MP days.

exhibits evident inhomogeneity and shows stronger intensity over regions with coastal topography, which is consistent with the results of Chen et al. (2016). In the afternoon, the rainfall is dominant on the inland area (Figs. 3e–g). Taking 113°E as the boundary, afternoon rainfall over western and eastern inland South China exhibits significantly different features (Fig. 5a). The eastern inland rainfall develops from moist convection that is initiated in the early-morning hours after sunrise over the northeastern PRD. It peaks in the early afternoon (~1400 LST), with a wider range compared with that in the morning, and dissipates in the late afternoon (Figs. 3c–g). The eastern inland rainfall is quasi-stationary, while the western inland rainfall is closely related to the southeastward propagation of rainbands initiated and developed from the windward side of the YGP (Figs. 3a–h and 5a), which migrate to South China near noon. After the movement of previously weakened rainfall belts, the western inland rainfall develops in the afternoon (Fig. 5a). The western inland rainfall peaks around 1600 LST and further migrates to central inland South China in the late afternoon (Figs. 3e–g and 5a). The inland rainfall gradually disappears after sunset (Fig. 3h).

(ii) During the AP days, little rainfall can be found from midnight to morning over South China (Figs. 3i–l). Rainfall initiates near noon over central and western inland South China and intensifies in the afternoon (Figs. 3m–o), with little offshore or inland propagation (Fig. 4b). The eastern inland rainfall is much weaker compared with that during the EAP days (Fig. 3). Rainfall peaks in the late afternoon over central and western inland South China, which is differ from the spatiotemporal pattern of afternoon rainfall during the EAP days. In addition, the speed of eastward

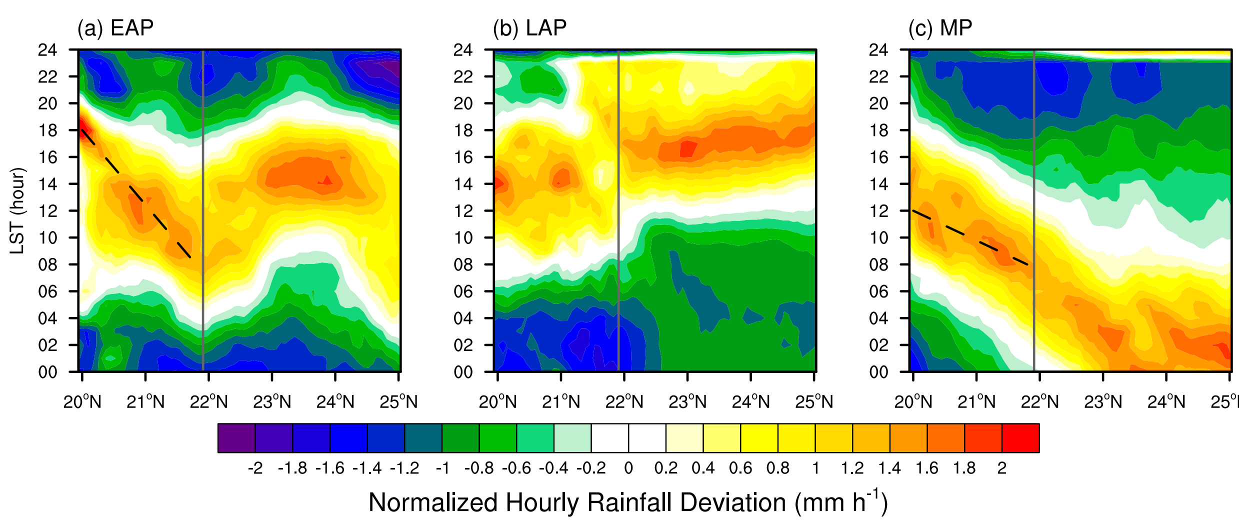

FIG. 4. Time–latitude Hovmöller diagrams of the normalized hourly rainfall deviation (mm h^{-1}) estimated as the mean precipitation rate at each hour minus the mean precipitation rate throughout the day, normalized by the standard deviation of hourly precipitation averaged from 111° to 117°E during the (a) EAP, (b) LAP, and (c) MP days. The gray solid lines represent the coastline.

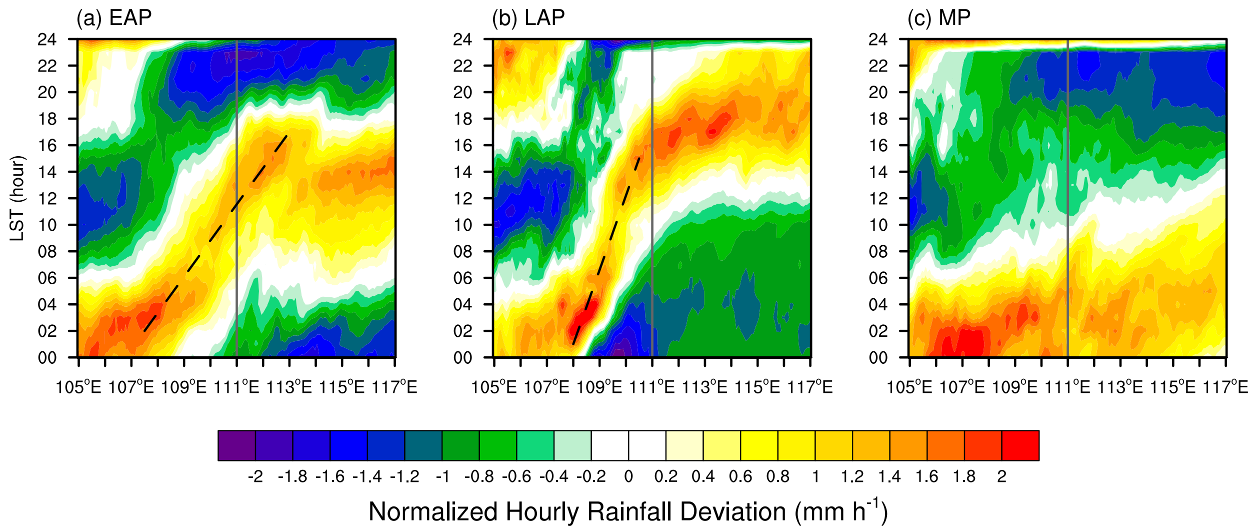

FIG. 5. Time–longitude Hovmöller diagrams of the normalized hourly rainfall deviation (mm h^{-1}) estimated as the mean precipitation rate at each hour minus the mean precipitation rate throughout the day, normalized by the standard deviation of hourly precipitation averaged from 21.5° to 26°N during the (a) EAP, (b) LAP, and (c) MP days. The gray solid lines represent the western boundary of South China.

propagation signal during the LAP days is much lower than that during the EAP days owing to much weaker magnitude of rainfall along the windward side of the YGP (Fig. 3) and could not enter South China during the afternoon (Fig. 5b). Based on the above analysis, the underlying mechanisms controlling the afternoon rainfall vary between the EAP and LAP modes, which will be further discussed in the next section.

(iii) During the MP days, rainfall initiates in the northeastern PRD and along the coast around midnight, similar to that during the EAP days (Fig. 3q). However, after the initiation stage, the features of rainfall become widely different. Rainfall over the northeastern PRD weakens after sunrise (Figs. 3q–t) and is much less pronounced compared with that during the EAP days. On the other hand, the intensity of offshore rainfall is stronger than that during the EAP days, which is more concentrated along the coastline (Figs. 3b–d). The coastal rainfall propagates offshore in the morning (Figs. 3s and 4b). After 0900 LST, the offshore rainfall becomes suppressed and continues propagating offshore (Fig. 3t). The coastal rainfall center is completely migrating into the northern SCS near midday (Fig. 3u) and gradually dissipates in the far offshore during the afternoon (Figs. 3u–w). The offshore propagation speed of rainfall is greater than 10 m s^{-1} and is much faster than that during the EAP days (Fig. 4). The afternoon inland rainfall is negligible during the MP days (Figs. 3u–w). In addition, rainfall belts also emerge on the windward side of YGP around midnight (Fig. 3q), which, however, maintain and finally dissipate in situ in the early morning (Fig. 5c).

In summary, three principle DCR modes over South China during the presummer rainy season are obtained by the EOF analysis: one early-afternoon rainfall mode (EAP), which features a double peaks, with a major peak at 1400 LST and a secondary peak at 0900 LST; one late-afternoon and one morning rainfall mode (LAP and MP), with a single peak in the late afternoon (~1800 LST) and early morning (~0300 LST), respectively. The underlying physical mechanisms controlling DCR associated with the above three modes follow in detail.

4. Mechanisms controlling the diurnal cycle of rainfall

a. The nocturnal–morning rainfall

As shown in section 3, significant nocturnal to morning rainfall occurs during both of the EAP and MP days which, however, exhibits considerably different features. During the EAP days, rainfall over the northeastern PRD is more pronounced, and the coastal rainfall is centered along the coastline. During the MP days, the offshore rainfall is stronger and the offshore propagating speed of rainfall is much faster than that during the EAP days (Figs. 3 and 4). These different phenomena can be attributed to the variety of the controlling mechanisms.

The large-scale conditions during the three DCR modes are illustrated in Fig. 6. At 500 hPa, westerly flows are prevailing over South China. A trough axis is located at the west of South China during the EAP days (Fig. 6a), which favors the intrusion of colder air. Such a trough is absent during the LAP and MP days (Figs. 6b,c), allowing less cold air to northern Guangxi with lower precipitation over the windward side of the YGP (Fig. 3). South China is controlled by the low-level southwesterly wind among all the three DCR modes, with the strongest ambient wind during the EAP days and the weakest during the MP days.

During the EAP days, associated with the most intense low-level southwesterly monsoonal wind, the nocturnal BLJs induced by inertial oscillations are pronounced over the

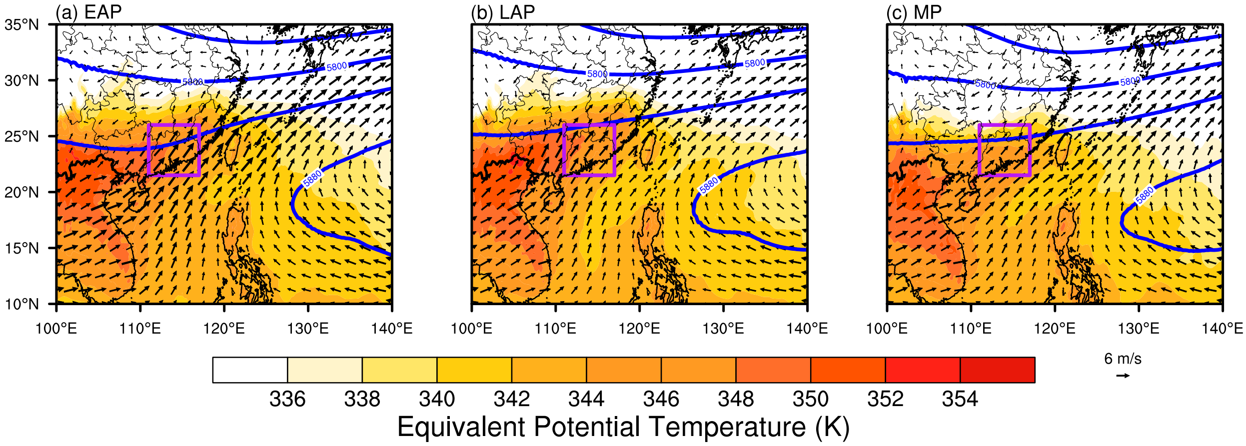

FIG. 6. Horizontal distributions of the daily mean 850-hPa equivalent potential temperature (shading; K), 850-hPa horizontal wind (vectors; m s^{-1}) and 500-hPa geopotential height (blue contours; gpm) during the (a) EAP, (b) LAP, and (c) MP days. The purple boxes show the domain of South China in this study.

northern SCS in the early morning (Fig. 7a), which play important roles in modulating the DCR over South China due to the enhanced moisture transport and the associated dynamic process (Xue et al. 2018; Du and Chen 2019b; Dong et al. 2021). The BLJ associated windward mechanical lifting is essential for the formation of nocturnal to morning rainfall over the northeastern PRD (Rao et al. 2019). Meanwhile, the differential surface friction across the coastline is believed to be the key factor for the initiation of rainfall along the coastline under the high ambient wind conditions (Chen et al. 2014, 2017). The 2-hourly evolution of the perturbation wind from 0000 to 0600 LST is displayed in Fig. 8. The daily mean wind has been subtracted to reveal the diurnal signal of coastal circulations more clearly. At 0000 LST, the coastal South China is dominated by the onshore perturbation wind in the low level (Fig. 8a), which is a combined signal of the residual sea breeze and the nocturnal enhanced low-level wind in response to the inertial oscillation (Blackadar 1957;

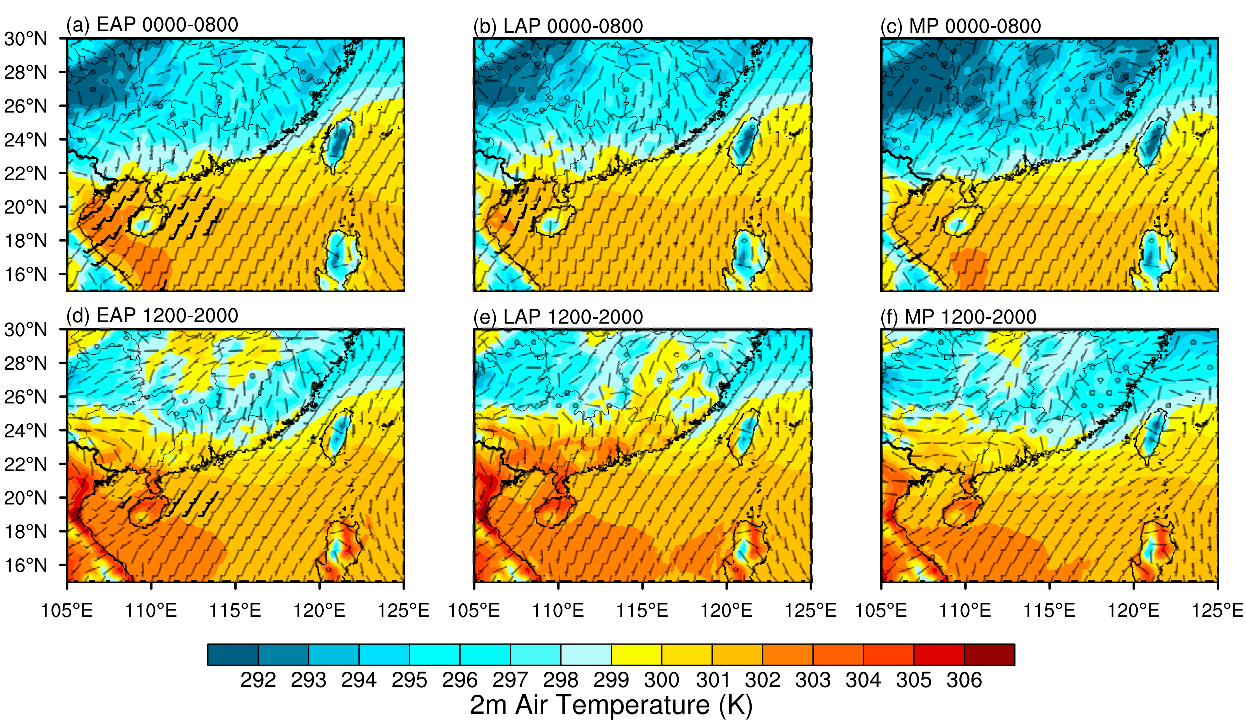

FIG. 7. Horizontal distributions of 2-m air temperature (shading; K) and horizontal wind barbs (a full barb is 8 m s^{-1}; bold black barbs for above 10 m s^{-1}) at 950 hPa averaged (top) from 0000 to 0800 LST and (bottom) from 1200 to 2000 LST during the (a),(d) EAP, (b),(e) LAP, and (c),(f) MP days.

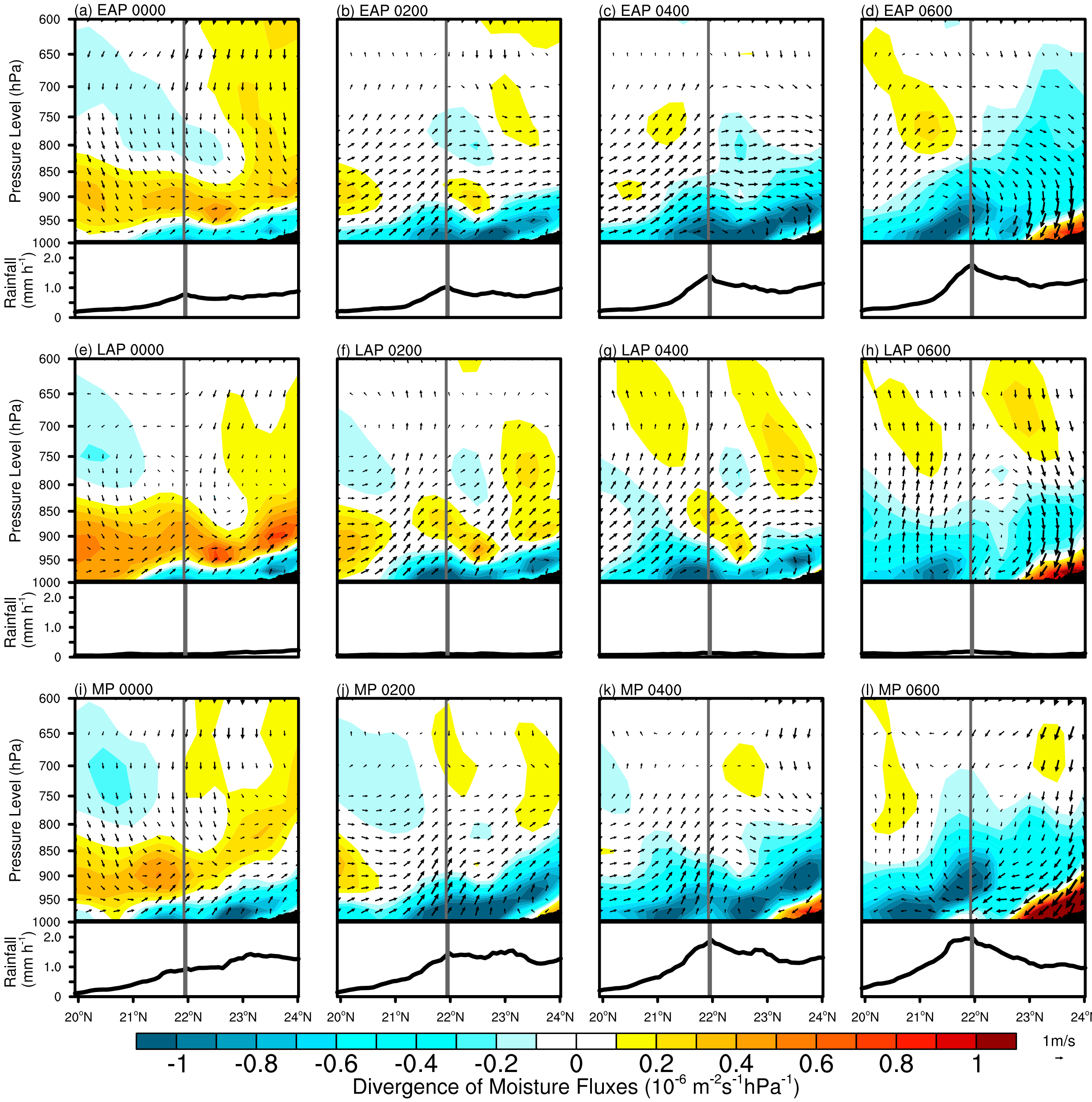

FIG. 8. Composite vertical cross sections of perturbation meridional wind (vectors; m s^{-1}), vertical wind (vectors; -50 Pa s^{-1}), and divergence of moisture fluxes (shading; 10^{-6} m^{-2} s^{-1} hPa^{-1}) with respect to their daily means and the latitude profile of hourly rainfall (mm h^{-1}) at (a),(e),(i) 0000, (b),(f),(j) 0200, (c),(q),(k) 0400, and (d),(h),(l) 0600 LST during the (top) EAP, (middle) LAP, and (bottom) MP days along the meridional direction averaged in the red box of Fig. 1a. The black shaded area shows the averaged terrain elevations. The gray solid lines indicate the coastline.

Chen et al. 2009, 2017; Xue et al. 2018). Strong onshore wind induces the convergence zone along the coastline because of the differential surface friction between land and ocean and facilitates the initiation of the coastal rainfall. The land breeze begins to establish after 0000 LST, but the onshore wind is still pronounced over the coastal region (Figs. 8b,c). The land-breeze circulations further strengthen and encounter with onshore monsoonal flow alone the coastline in the early morning, which enhanced the coastal rainfall (Fig. 8d). The land breeze exhibits little offshore extension in the morning during the EAP days, which is suppressed by the high background monsoonal wind (Figs. 6a and 7a; Chen et al. 2017). Therefore, the coastal rainfall center maintains along the coastline until noon. With the retreating of the land breeze and the establishment of the sea breeze, the coastal rainfall center vanishes in the afternoon (Figs. 3e–h).

For the MP days, however, the low-level monsoonal wind is weaker (Figs. 6 and 7). The BLJs over the northern SCS are absent. Therefore, rainfall over the northeastern PRD, which is highly influenced by the intensity of low-level ambient wind (Rao et al. 2019), is weaker than that during the EAP days (Fig. 3). The coastal rainfall center emerges along the coastline after 0200 LST, associated with the establishment of the land breeze (Figs. 3q–s and 8j). The convergence line between the land breeze and onshore monsoon wind favors the formation of coastal center in the early morning (Figs. 8i–k). The intensity of the land breeze during the MP days is stronger than that during the EAP days (Fig. 8) due to the larger land–sea thermal contrast (Figs. 7a,c). Such a strong land breeze enhances the coastal lifting and induces more intense coastal early-morning rainfall than that during the EAP days (Figs. 3 and 8). The coastal center further migrates to near offshore at 0600 LST owing to the offshore expansion of the land breeze (Figs. 3s and 8l). The offshore expansion of the land breeze under the MP mode is more pronounced than that under the EAP mode because of the relatively weak ambient monsoonal wind (Figs. 6 and 7; Chen et al. 2017).

Furthermore, as mentioned in section 3, both coastal rainfall during the EAP and MP days propagates offshore in the morning, but with different propagating speed (Fig. 4). Previous studies documented that the offshore propagation of rainfall is largely affected by the gravity wave (Mapes et al. 2003; Aves and Johnson 2008; Du and Rotunno 2018; Bai et al. 2020). The offshore propagation speed during the MP days is much higher than that during the EAP days (Fig. 4). Such a difference could be related to the intensity of background wind. The background wind changes the pattern of the gravity waves and further affects the propagation speed owing to the effects of Doppler shift (Qian et al. 2009; Du and Rotunno 2018). The onshore ambient wind is much stronger during the EAP days (Fig. 6), inducing the lower offshore propagation speed compared with that during the MP days. To further verify the effects of background wind on the offshore propagation of rainfall, we have classified the presummer days into weak-wind days (lowest 30% of low-level wind speeds), strong-wind days (highest 30% of low-level wind speeds), and moderate-wind days (all other wind events) according to the averaged daily mean low-level (from the surface to 850 hPa) wind speed over South China and northern SCS (18°–26°N, 111°–117°E). During the strong-wind days, the offshore propagation speed of rainfall is similar to that during the EAP days. However, the offshore propagation speed is higher with the weaker ambient wind and the offshore propagation speed during the weak-wind days is comparable to that during the MP days (Figs. S1 and S2 in the online supplemental material). The above analysis further validates the important role of the intensity of the background wind in the offshore propagation of rainfall. The mesoscale features of gravity wave and its impacts on the DCR during the different DCR modes will be further examined via high-resolution models in the future.

With respect to the LAP days, the land-breeze circulation is also pronounced, whereas the coastal rainfall is relatively weak (Figs. 3i–p and 8e–h). Such a weak coastal rainfall could result from the unfavorable moisture convergence conditions in the early morning (Fig. S3b). Thus, the offshore propagation signal is negligible (Fig. 4b). It is worth noting that the mountain–plain solenoid (MPS) produced by the coastal terrain can combine with the land breeze and enhance the offshore propagation of rainfall (Chen et al. 2016). However, in this study it is currently not sufficient to identify the effects of the MPS and land breeze on DCR separately due to the coarse resolution, which needs to be further examined based on high-resolution model output in the future.

In summary, nocturnal to morning rainfall centers along the coastline during the EAP days, while the offshore rainfall is stronger during the MP days. Convergence zone induced by the strong onshore wind due to the differential surface friction between land and ocean is responsible for the initiation of coastal rainfall during the EAP days. This convergence zone would be enhanced by land breeze encountering with ambient onshore wind and produces stronger rainfall along the coastline in the early morning. The formation of coastal rainfall is closely related to the establishment of the land breeze during the MP days, which is stronger than that during the EAP days. The offshore expansions of land breeze, which are weak during the EAP days, favor the development of offshore rainfall during the MP days. In addition, the offshore propagation speed varies between the EAP and MP modes, with the MP faster, due to the different intensity of background wind.

b. *The afternoon rainfall*

The convective instability of atmospheric conditions is an important factor impacting the afternoon rainfall over South China (Luo et al. 2013; Chen et al. 2014) and can be determined by the convective available potential energy (CAPE; Chen et al. 2014; Du et al. 2022). The intensity of afternoon CAPE is different among the three DCR modes, showing the highest values during the LAP days and the lowest ones during the MP days (Figs. 9d–f). Such difference can also be found from midnight to morning (Figs. 9a–c), but the magnitude is much weaker compared to the afternoon. Due to the release of unstable energy in the morning and the increased cloud cover (Wang et al. 2021), the CAPE over South China exhibits little enhancement in the afternoon during the EAP and MP days. The different magnitude of CAPE is closely related to the different surface temperature among the three DCR modes. Higher temperature tends to contain more water vapor (not shown) and facilitates more unstable conditions which are easier to trigger rainfall (Figs. 7d–f).

In addition, the dynamic lifting conditions are another important factor to modulate the afternoon rainfall (Jiang et al. 2017; Chen et al. 2018). The favorable lifting conditions are necessary to overcome the convective inhibition for the growth of convection. The perturbation vertical motion and vorticity with respect to their daily means are illustrated in Fig. 10. During the EAP days, South China is generally controlled by the rising motion from the morning to late afternoon

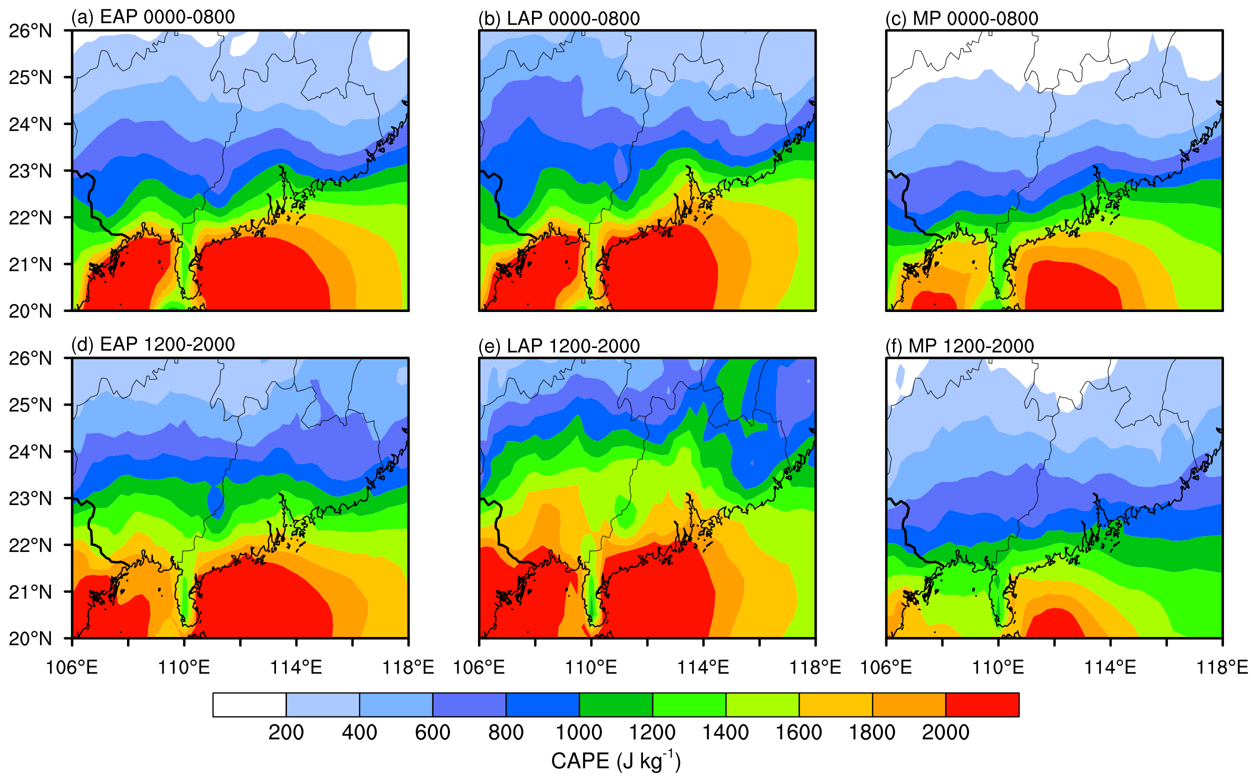

FIG. 9. Horizontal distributions of CAPE (J kg^{-1}) averages (top) from 0000 to 0800 LST and (bottom) 1200 to 2000 LST during the (a),(d) EAP, (b),(e) LAP, and (c),(f) MP days.

(Figs. 10a–d). The rising motion maximums around 114°N in the morning (Fig. 10b), coinciding well with the rainfall maximum around the northeastern PRD (Figs. 3c,d). The upward vertical velocity reaches the peak in the early afternoon, showing more intense motions over the eastern inland South China. However, the upward motion is weaker in the late afternoon and the motion maximum migrates to the western inland South China (Fig. 10d). During the LAP days, South China is dominated by the upward motion in the afternoon, which is more pronounced over western South China in the late afternoon (Figs. 10e–h). It is noteworthy that for the MP days, the upward motion peaks near 114°E in the morning, but maximums around 117°E in the afternoon (Figs. 10i–l). Such an upward motion maximum coincides well with the rainfall center over northeastern PRD in the early morning, which gradually weakens and moves eastward from morning to afternoon (Figs. 3s–v and 5c).

The thermal–dynamic conditions during both of the EAP and LAP days are favorable for the initiation and development of afternoon rainfall (Figs. 9 and 10). However, as discussed in section 3, the spatiotemporal distributions and underlying mechanisms are different. The vorticity field exhibits two afternoon maximums over South China during the EAP days, coincides with the two rainfall centers as the western part peaked in the late afternoon and eastern part peaked in the early afternoon, respectively (Figs. 10c,d). The eastern inland rainfall develops from moist convection initiated in the early morning after sunrise and reaches maximums in the early afternoon (Figs. 3a–f and 5a). The eastern inland rainfall is dissipated after 1400 LST due to the weakened moisture supply (Fig. S3a) and consuming of unstable energy (Fig. 9d). The western inland rainfall is affected by the eastward propagation of rainfall belts originated from the windward side of the YGP around midnight, which is associated with the local instability conditions (Figs. 9 and 10). Such rainfall belts strengthen in the early morning due to the nocturnal enhanced low-level wind and start to weaken shortly after sunrise (Figs. 3a–d). The eastward-propagating rainfall enters into South China and reaches the weakest at around noon (Figs. 3e and 5a). While the eastward-propagating rainfall weakens, it appears to facilitate the subsequent formation of rainfall over western South China in the early afternoon (Figs. 3f and 5a), which are initiated along cold outflow boundaries as they occur from the previously weakened rainfall belts (Jiang et al. 2017). These are also demonstrated by analyses on diurnal variations of vorticity. The western positive vorticity zone originates from the windward side of the YGP near midnight (Figs. 10a and 11a). After the initiation stage, such a high positive vorticity zone propagates eastward, following the midtropospheric mean flow, and enters South China near noon, being consistent with the eastward propagation signal of rainfall (Fig. 5a). The diurnal cycles of vorticity fields further validate the eastward-propagating rainfall

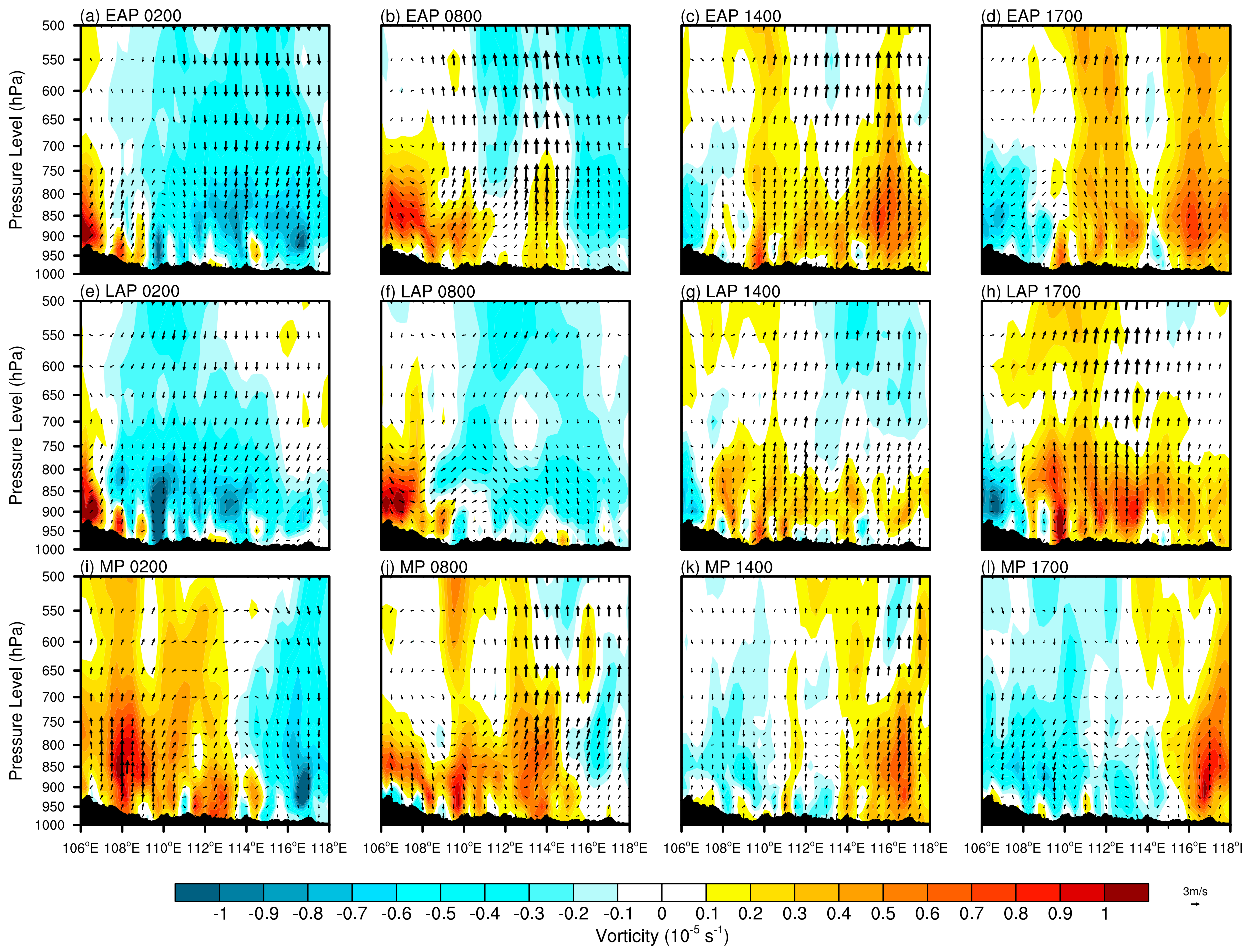

FIG. 10. Composite vertical cross sections of the perturbation zonal wind (vectors, m s^{-1}), vertical wind (vectors; -50 Pa s^{-1}) and vorticity (shading; 10^{-5} s^{-1}) with respect to their daily means at (a),(e),(i) 0200, (b),(f),(j) 0800, (c),(g),(k) 1400, and (d),(h),(l) 1700 LST during the (top) EAP, (middle) LAP, and (bottom) MP days along the zonal direction averaged in the red box of Fig. 1a. The black shaded area shows the averaged terrain elevations.

episodes associated with frontal activities, as mentioned in previous studies (Jiang et al. 2017; Dong et al. 2021).

During the LAP days, the eastern inland rainfall is negligible from morning to afternoon due to the unfavorable thermal–dynamic conditions and the lack of moisture supply. The speed of eastward propagation of rainfall is much lower during the LAP days compared with that during the EAP days, and it could not enter South China in the afternoon (Figs. 5b and 11b). Therefore, the western and central inland rainfall initiates locally (Fig. 3b), with little influenced by the eastward propagation of rainfall, and could be mainly influenced by the local convective instability and dynamic lifting conditions (Figs. 9 and 10). In addition, there is little afternoon rainfall during the MP days because of the unfavorable environment conditions (Figs. 9f and 10e–h) and the quasi-stationarity of rainfall initiated at the windward side of the YGP (Figs. 5c and 11c).

In general, the afternoon rainfall during the EAP days is mainly affected by the local instability and dynamic lifting conditions, eastward propagation of rainfall from windward side of the YGP and local moist convection initiated in the early morning. Yet the local instability and dynamic lifting conditions are the major factors controlling the afternoon rainfall during the LAP days.

5. Summary and discussion

In this study, the principal modes of DCR over South China during the presummer rainy season are investigated using the 23-yr satellite observations and reanalysis data. Three distinctly different DCR modes are identified based on the EOF analysis, that is, the early-afternoon precipitation (EAP) mode, the late-afternoon precipitation (LAP) mode, and the morning precipitation (MP) mode. The main findings are summarized below, which are also displayed in the schematics (Fig. 12):

1) For the EAP (Figs. 12a,b) mode, rainfall exhibits two diurnal peaks, with a major early-afternoon peak and a secondary morning peak. Rainfall starts to increase around midnight, reaches its peak at 1400 LST, and afterward

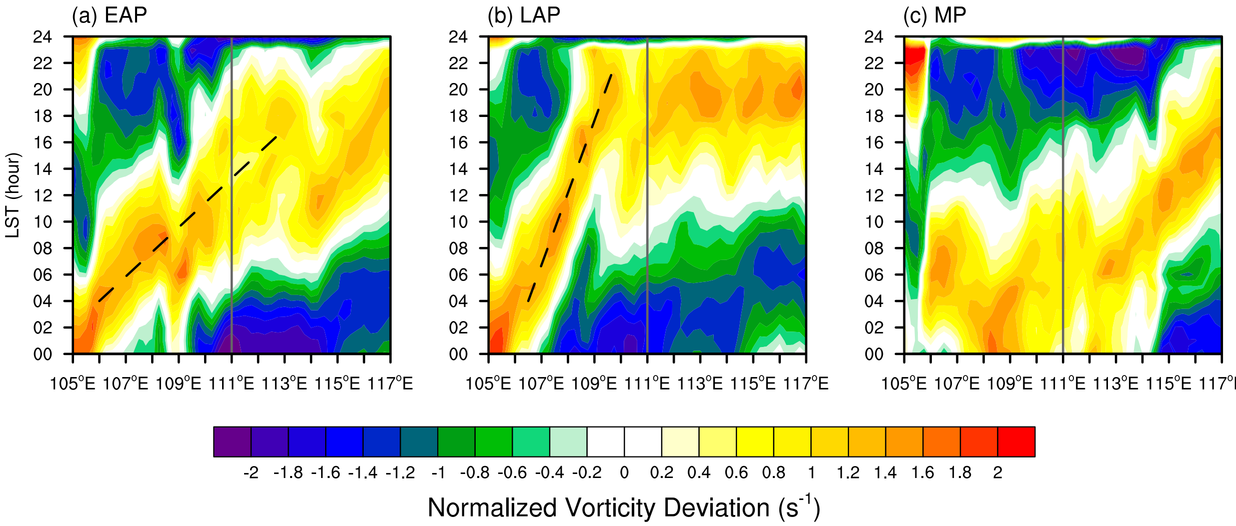

FIG. 11. Time–longitude Hovmöller diagrams of the normalized hourly 850-hPa vorticity deviation (s^{-1}) estimated as the vorticity at each hour minus the mean vorticity throughout the day, normalized by the standard deviation of hourly vorticity averaged from 21.5° to 26°N during the (a) EAP, (b) LAP, and (c) MP days. The gray solid lines indicate the western boundary of South China.

decreases to the minimum at midnight. The nocturnal to morning rainfall centers at the northeastern PRD and along the coastline. The coastal rainfall is initiated by the convergence line around midnight, which is caused by different friction between land and ocean under the high ambient wind conditions. The development of the land breeze further enhances the coastal rainfall in the early morning. Coastal rainfall propagates offshore in the morning with a relatively low speed. The morning precipitation centered over the northeastern PRD could be attributed to the BLJ-induced windward-side mechanical lifting. The afternoon rainfall dominates the inland area, which could be divided into eastern and western parts due to the different diurnal variations. The eastern inland rainfall develops from moist convection initiated in the early morning over northeastern PRD and reaches maximum in the early afternoon with the favorable thermal–dynamic and moisture conditions. On the other hand, the southeastward propagation of rainfall and associated frontal activities are responsible for the formation of western inland afternoon rainfall, which peaks in the late afternoon.

2) The LAP (Figs. 12c,d) mode features a late-afternoon peak (~1800 LST) and shows its minimum in the early morning. Afternoon rainfall under this mode is pronounced over the western part of inland South China. The thermal instability and dynamic lifting conditions jointly favor the formation of afternoon rainfall. The eastward-propagating rainfall shows little impact on the afternoon rainfall, which is different from that under the EAP mode. It is because the eastward propagation of rainfall is much slower and could not enter South China in the afternoon. In addition, the nocturnal to morning rainfall is less pronounced owing to the unfavorable environment conditions.

3) The MP (Figs. 12e,f) mode exhibits a single peak in the early morning (~0300 LST) and disappears in the afternoon. The nocturnal to morning precipitation centers are located at the northeastern PRD and near-offshore region. Rainfall over the northeastern PRD is less pronounced than that under the EAP mode due to the weaker low-level monsoonal wind. The near offshore rainfall is induced by the convergence between the low-level onshore wind and the land breeze, which exhibits pronounced offshore expansions in the early morning. It migrates to far offshore in the morning, with a faster speed than that under the EAP mode due to the weaker ambient wind. In the afternoon, the thermal–dynamic conditions are unfavorable for the rainfall formation.

It should be noted that the EOF1 mode exhibits a major and secondary peak around 0900 and 1400 LST, respectively. Such a diurnal feature is different with the DCR during the presummer days (Fig. 1b), which exhibits double peaks feature, with the major peak at 1600 LST. During the EAP days, the low-level southwesterly winds are strongest among the above three modes, with the pronounced boundary layer jet located over northern SCS (Figs. 6 and 7). As shown in previous studies (Rao et al. 2019), the strong-wind conditions are favorable for the formation of the early-afternoon rainfall peak over South China. Moreover, the near-noon rainfall minimum vanishes during the strong-wind conditions, because the strong low-level wind transports abundant warm–moist air into South China, which could cover the near-noon rainfall minimum (Fig. S3a). Rainfall increases from midnight to early afternoon during the EAP days. After 0300 LST, the rainfall decreases corresponding to the weakened moisture transportation (Fig. S3a) and the consuming of unstable energy (Fig. 9). Therefore, the formation of early-afternoon rainfall during the EAP days is related to the high ambient winds and the associated abundant moisture transportation.

To further verify such features, we divide the presummer days into strong-, moderate-, and weak-wind days (details are

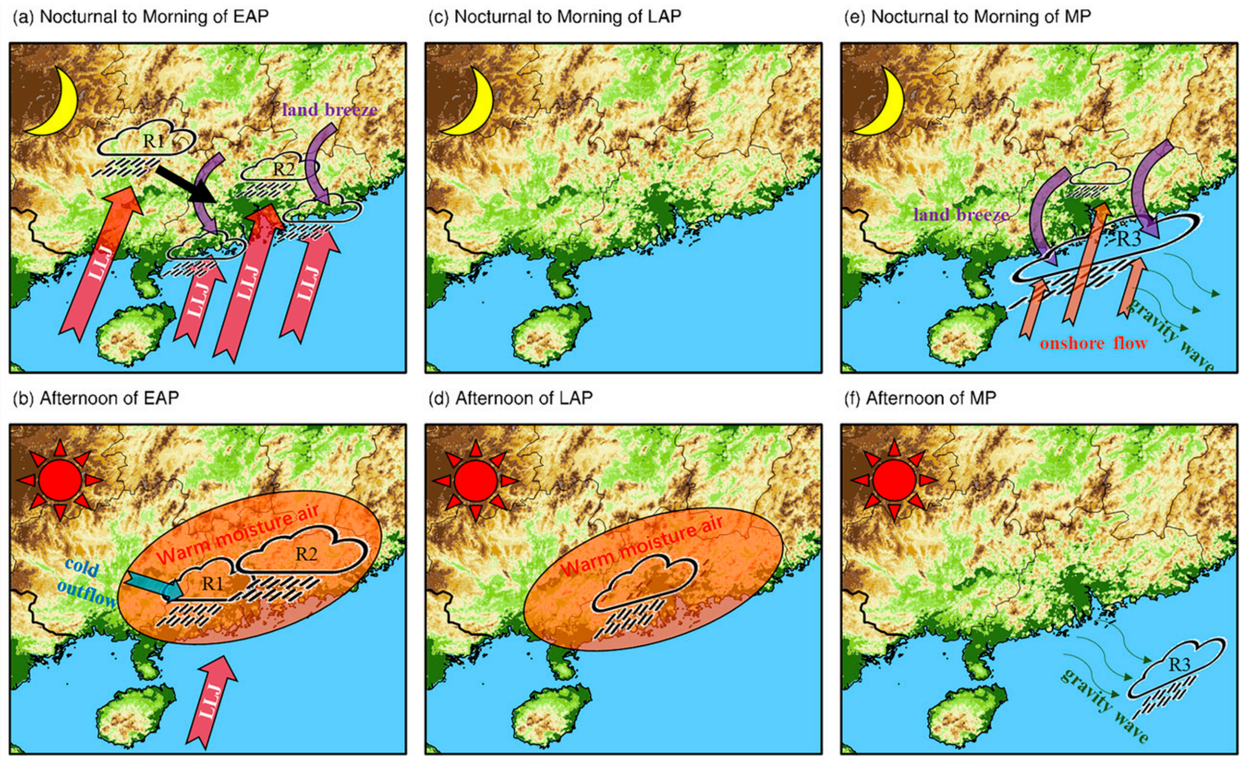

FIG. 12. Schematic diagrams of the joint impacts of topography, LLJs, land breeze, gravity wave, cold outflow, and warm moist airmass on DCR over South China under the (a),(b) EAP, (c),(d) LAP, and (e),(f) MP modes. The text "R1" indicates the eastward-propagating rainfall in (a) and rainfall effected by the eastward-propagating rainbands in (b). The text "R2" refers to the eastern part of rainfall over inland South China, which initiates at northeastern PRD in the morning in (a) and further develops in the early afternoon in (b). The text "R3" denotes the offshore propagating rainfall in (e) and (f).

shown in section 4a). Fig. S4 illustrates the DCR during the strong-wind, moderate-wind and weak-wind days, respectively. During the strong-wind days, the DCR is similar to that during the EAP days (Figs. S3a and S4a) because such two periods both exhibit intense low-level wind. Rainfall shows a major peak in the early afternoon during the strong-wind days. During the moderate- and weak-wind days, rainfall exhibits a late-afternoon peak, with a near-noon decreasing (at around 1000 LST) more obvious than that during the strong-wind days (Fig. S4). Rainfall during the strong-wind days accounts for the majority of rainfall during the presummer days, especially over the northeastern PRD and coastal area (Fig. S5a). Therefore, the DCR during the EAP days is considered as the major pattern in presummer. In addition, LLJs are pronounced during the presummer rainy season and are important for the initiation and development of presummer rainfall (Chen et al. 2014; Du and Chen 2019a,b; Zhang and Meng 2019; Rao et al. 2019; Dong et al. 2021). The EOF1 mode well captures the features of LLJs and is therefore demonstrated reliable.

Previous studies have usually examined the DCR over South China under different synoptic forcings (Chen et al. 2017; Wang et al. 2021; Dong et al. 2021). On that basis, this study provides a new perspective in objectively classifying the DCR episodes. Furthermore, some new knowledges are added to the study of DCR over South China. In particular, the afternoon rainfall over South China exhibits significantly regional diversity, with a variety of controlling mechanisms. Such a spatial discrepancy has seldom been mentioned in previous literature. In addition, this study confirms the eastward-propagating rainfall episodes and associated frontal activities, which has been proposed as a hypothesis in previous studies (Jiang et al. 2017; Dong et al. 2021). On the other hand, the DCR over South China and its associated thermodynamics are examined using a relatively coarse dataset. Further studies will be performed using high-resolution models to gain additional insights into the underlying mesoscale processes, such as the land and sea breeze, mountain–plain solenoid, low-level jets, gravity waves, and the effects of topography. Moreover, the long-term variations of DCR under the three DCR modes also deserve further investigation.

Acknowledgments. The authors are grateful to three anonymous reviewers and Editor Dr. Hisashi Nakamura for the valuable comments and suggestions. This study was supported by the National Key Research and Development Project of China (Grant 2017YFC1502002), the project of Fujian Key Laboratory of Severe Weather (2020KFKT02), the Postgraduate Research and Practice Innovation Program of Jiangsu Province (Grant KYCX22_1144), the research project of Jiangsu Meteorological

Bureau (Grant KQ202209), the Basic Research Fund of Chinese Academy of Meteorological Sciences (Grant 2022Y027), the National Natural Science Foundation of China (Grant 91937301 and 42205162), and the China Scholarship Council (Grant 202209040016).

Data availability statement. The CMORPH global precipitation dataset can be downloaded online (https://rda.ucar.edu/), and the ERA5 reanalysis data are available online (https://cds.climate.copernicus.eu/cdsapp#!/home).

REFERENCES

Aves, S. L., and R. H. Johnson, 2008: The diurnal cycle of convection over the northern South China Sea. *J. Meteor. Soc. Japan*, **86**, 919–934, https://doi.org/10.2151/jmsj.86.919.

Bai, L., G. Chen, and L. Huang, 2020: Convection initiation in monsoon coastal areas (South China). *Geophys. Res. Lett.*, **47**, e2020GL087035, https://doi.org/10.1029/2020GL087035.

——, ——, Y. Huang, and Z. Meng, 2021: Convection initiation at a coastal rainfall hotspot in South China: Synoptic patterns and orographic effects. *J. Geophys. Res. Atmos.*, **126**, e2021JD034642, https://doi.org/10.1029/2021JD034642.

Blackadar, A. K., 1957: Boundary layer wind maxima and their significance for the growth of nocturnal inversions. *Bull. Amer. Meteor. Soc.*, **38**, 283–290, https://doi.org/10.1175/1520-0477-38.5.283.

Cai, S., A. Huang, K. Zhu, B. Yang, X. Yang, Y. Wu, and X. Mu, 2021: Diurnal cycle of summer precipitation over the eastern Tibetan Plateau and surrounding regions simulated in a convection-permitting model. *Climate Dyn.*, **57**, 611–632, https://doi.org/10.1007/s00382-021-05729-5.

Chen, G., W. Sha, and T. Iwasaki, 2009: Diurnal variation of precipitation over southeastern China: 2. Impact of the diurnal monsoon variability. *J. Geophys. Res.*, **114**, D21105, https://doi.org/10.1029/2009JD012181.

——, ——, M. Sawada, and T. Iwasaki, 2013: Influence of summer monsoon diurnal cycle on moisture transport and precipitation over eastern China. *J. Geophys. Res. Atmos.*, **118**, 3163–3177, https://doi.org/10.1002/jgrd.50337.

——, R. Lan, W. Zeng, H. Pan, and W. Li, 2018: Diurnal variations of rainfall in surface and satellite observations at the monsoon coast (South China). *J. Climate*, **31**, 1703–1724, https://doi.org/10.1175/JCLI-D-17-0373.1.

——, Y. Du, and Z. Wen, 2021: Seasonal, interannual and interdecadal variations of the East Asian summer monsoon: A diurnal-cycle perspective. *J. Climate*, **34**, 4403–4421, https://doi.org/10.1175/JCLI-D-20-0882.1.

Chen, X. C., K. Zhao, and M. Xue, 2014: Spatial and temporal characteristics of warm season convection over Pearl River Delta region, China, based on 3 years of operational radar data. *J. Geophys. Res. Atmos.*, **119**, 12 447–12 465, https://doi.org/10.1002/2014JD021965.

——, ——, ——, B. Zhou, X. Huang, and W. Xu, 2015: Radar observed diurnal cycle and propagation of convection over the Pearl River Delta during mei-yu season. *J. Geophys. Res. Atmos.*, **120**, 12 557–12 575, https://doi.org/10.1002/2015JD023872.

——, F. Zhang, and K. Zhao, 2016: Diurnal variations of the land–sea breeze and its related precipitation over South China. *J. Atmos. Sci.*, **73**, 4793–4815, https://doi.org/10.1175/JAS-D-16-0106.1.

——, ——, and ——, 2017: Influence of monsoonal wind speed and moisture content on intensity and diurnal variations of the mei-yu season coastal rainfall over South China. *J. Atmos. Sci.*, **74**, 2835–2856, https://doi.org/10.1175/JAS-D-17-0081.1.

Dai, A., 2001: Global precipitation and thunderstorm frequencies. Part II: Diurnal variations. *J. Climate*, **14**, 1112–1128, https://doi.org/10.1175/1520-0442(2001)014<1112:GPATFP>2.0.CO;2.

——, and K. E. Trenberth, 2004: The diurnal cycle and its depiction in the community climate system model. *J. Climate*, **17**, 930–951, https://doi.org/10.1175/1520-0442(2004)017<0930:TDCAID>2.0.CO;2.

——, F. Giorgi, and K. E. Trenberth, 1999: Observed and model simulated precipitation diurnal cycle over the contiguous United States. *J. Geophys. Res.*, **104**, 6377–6402, https://doi.org/10.1029/98JD02720.

Ding, Y., 1992: Summer monsoon rainfalls in China. *J. Meteor. Soc. Japan*, **70**, 373–396, https://doi.org/10.2151/jmsj1965.70.1B_373.

Dong, F., X. Zhi, L. Zhang, and C. Ye, 2021: Diurnal variations in coastal boundary layer jets over the northern South China Sea and their impacts on diurnal cycle of rainfall over southern China during the early-summer rainy season. *Mon. Wea. Rev.*, **149**, 3341–3363, https://doi.org/10.1175/MWR-D-20-0292.1.

Du, Y., and R. Rotunno, 2018: Diurnal cycle of rainfall and winds near the south coast of China. *J. Atmos. Sci.*, **75**, 2065–2082, https://doi.org/10.1175/JAS-D-17-0397.1.

——, and G. Chen, 2019a: Heavy rainfalls associated with double low-level jets over southern China. Part II: Convection initiation. *Mon. Wea. Rev.*, **147**, 543–565, https://doi.org/10.1175/MWR-D-18-0102.1.

——, and ——, 2019b: Climatology of low-level jets and their impact on rainfall over southern China during the early-summer rainy season. *J. Climate*, **32**, 8813–8833, https://doi.org/10.1175/JCLI-D-19-0306.1.

——, Q. Zhang, Y.-L. Chen, Y. Zhao, and X. Wang, 2014: Numerical simulations of spatial distributions and diurnal variations of low-level jets in China during early summer. *J. Climate*, **27**, 5747–5767, https://doi.org/10.1175/JCLI-D-13-00571.1.

——, Y. A. Shen, and G. X. Chen, 2022: Influence of coastal marine boundary layer jets on rainfall in South China. *Adv. Atmos. Sci.*, **39**, 782–801, https://doi.org/10.1007/s00376-021-1195-7.

Hersbach, H., and Coauthors, 2020: The ERA5 global reanalysis. *Quart. J. Roy. Meteor. Soc.*, **146**, 1999–2049, https://doi.org/10.1002/qj.3803.

Huang, S. S., 1986: *The Heavy Rain during the Pre-summer Period over Southern China* (in Chinese). Guangdong Technology Press, 244 pp.

Jiang, Z., D.-L. Zhang, R. Xia, and T. Qian, 2017: Diurnal variations of presummer rainfall over southern China. *J. Climate*, **30**, 755–773, https://doi.org/10.1175/JCLI-D-15-0666.1.

Joyce, R. J., J. E. Janowiak, P. A. Arkin, and P. Xie, 2004: CMORPH: A method that produces global precipitation estimates from passive microwave and infrared data at high spatial and temporal resolution. *J. Hydrometeor.*, **5**, 487–503, https://doi.org/10.1175/1525-7541(2004)005<0487:CAMTPG>2.0.CO;2.

Kikuchi, K., and B. Wang, 2008: Diurnal precipitation regimes in the global tropics. *J. Climate*, **21**, 2680–2696, https://doi.org/10.1175/2007JCLI2051.1.

Li, J., R. C. Yu, and T. J. Zhou, 2008: Seasonal variation of the diurnal cycle of rainfall in southern contiguous China. *J. Climate*, **21**, 6036–6043, https://doi.org/10.1175/2008JCLI2188.1.

Li, P., K. Furtado, T. Zhou, H. Chen, J. Li, Z. Guo, and C. Xiao, 2018: The diurnal cycle of East Asian summer monsoon precipitation simulated by the met office unified model at convection-permitting scales. *Climate Dyn.*, **55**, 131–151, https://doi.org/10.1007/s00382-018-4368-z.

Luo, Y., H. Wang, R. Zhang, W. Qian, and Z. Luo, 2013: Comparison of rainfall characteristics and convective properties of monsoon precipitation systems over South China and the Yangze and Huai River basin. *J. Climate*, **26**, 110–132, https://doi.org/10.1175/JCLI-D-12-00100.1.

Mapes, B. E., T. T. Warner, and M. Xu, 2003: Diurnal patterns of rainfall in northwestern South America. Part III: Diurnal gravity waves and nocturnal convection offshore. *Mon. Wea. Rev.*, **131**, 830–844, https://doi.org/10.1175/1520-0493(2003)131<0830:DPORIN>2.0.CO;2.

Qian, T., C. C. Epifanio, and F. Zhang, 2009: Linear theory calculations for sea breeze in a background wind: The equatorial case. *J. Atmos. Sci.*, **66**, 1749–1763, https://doi.org/10.1175/2008JAS2851.1.

Rao, X., K. Zhao, X. Chen, A. Huang, M. Xue, Q. Zhang, and M. Wang, 2019: Influence of synoptic pattern and low-level wind speed on intensity and diurnal variations of orographic convection in summer over Pearl River Delta, South China. *J. Geophys. Res. Atmos.*, **124**, 6157–6179, https://doi.org/10.1029/2019JD030384.

Stensrud, D. J., 1996: Importance of low-level jets to climate: A review. *J. Climate*, **9**, 1698–1711, https://doi.org/10.1175/1520-0442(1996)009<1698:IOLLJT>2.0.CO;2.

Su, L., J. C. H. Fung, J. Li, and W. K. Wong, 2021: Trends in diurnal cycle of summertime rainfall over coastal South China in the past 135 years: Characteristics and possible causes. *J. Geophys. Res. Atmos.*, **126**, e2020JD033621, https://doi.org/10.1029/2020JD033621.

Wallace, J. M., 1975: Diurnal variations in precipitation and thunderstorm frequency over the conterminous United States. *Mon. Wea. Rev.*, **103**, 406–419, https://doi.org/10.1175/1520-0493(1975)103<0406:DVIPAT>2.0.CO;2.

Wang, B., H.-J. Kim, K. Kikuchi, and A. Kitoh, 2011: Diagnostic metrics for evaluation of annual and diurnal cycles. *Climate Dyn.*, **37**, 941–955, https://doi.org/10.1007/s00382-010-0877-0.

Wang, C., K. Zhao, A. Huang, X. Chen, and X. Rao, 2021: The crucial role of synoptic pattern in determining the spatial distribution and diurnal cycle of heavy rainfall over the South China coast. *J. Climate*, **34**, 2441–2458, https://doi.org/10.1175/JCLI-D-20-0274.1.

Xue, M., X. Luo, K. Zhu, Z. Sun, and J. Fei, 2018: The controlling role of boundary layer inertial oscillations in meiyu frontal precipitation and its diurnal cycles over China. *J. Geophys. Res. Atmos.*, **123**, 5090–5115, https://doi.org/10.1029/2018JD028368.

Yang, G.-Y., and J. Slingo, 2001: The diurnal cycle in the tropics. *Mon. Wea. Rev.*, **129**, 784–801, https://doi.org/10.1175/1520-0493(2001)129<0784:TDCITT>2.0.CO;2.

Yu, R., Y. Xu, T. Zhou, and J. Li, 2007a: Relation between rainfall duration and diurnal variation in the warm season precipitation over central eastern China. *Geophys. Res. Lett.*, **34**, L13703, https://doi.org/10.1029/2007GL030315.

——, T. Zhou, A. Xiong, Y. Zhu, and J. Li, 2007b: Diurnal variations of summer precipitation over contiguous China. *Geophys. Res. Lett.*, **34**, L01704, https://doi.org/10.1029/2006GL028129.

Yuan, W., R. Yu, M. Zhang, W. Lin, H. Chen, and J. Li, 2012: Regimes of diurnal variation of summer rainfall over subtropical East Asia. *J. Climate*, **25**, 3307–3320, https://doi.org/10.1175/JCLI-D-11-00288.1.

Zhang, L., L. Song, S. Zhu, Z. Guo, H. Wang, L. Zhou, C. Chen, and X. Zhi, 2022: Forecasts of the warm-sector heavy rainfall with a warm shear pattern over coastal areas of the Yangtze–Huaihe River in a regional business forecast model. *Front. Earth Sci.*, **10**, 938336, https://doi.org/10.3389/feart.2022.938336.

Zhang, M., and Z. Meng, 2019: Warm-sector heavy rainfall in southern China and its WRF simulation evaluation: A low-level-jet perspective. *Mon. Wea. Rev.*, **147**, 4461–4480, https://doi.org/10.1175/MWR-D-19-0110.1.